EPJ Photovoltaics **14**, 16 (2023)

https://doi.org/10.1051/epjpv/2023007

Special Issue on 'WCPEC-8: State of the Art and Developments in Photovoltaics', edited by Alessandra Scognamiglio, Robert Kenny, Shuzi Hayase and Arno Smets

Available online at: www.epj-pv.org

REGULAR ARTICLE

OPEN ACCESS

Laser-based monolithic series interconnection of two-terminal perovskite-CIGSe tandem solar cells: determination of the optimal scribe line properties

Christof Schultz[1,a,*], Guillermo Antonio Farias Basulto[2,a], Nicolas Otto[1], Janardan Dagar[3], Andreas Bartelt[1], Rutger Schlatmann[1,2], Eva Unger[3] and Bert Stegemann[1]

[1] HTW Berlin—University of Applied Sciences, Wilhelminenhofstr. 75a, 12459 Berlin, Germany
[2] Competence Centre Photovoltaics Berlin (PVcomB), Helmholtz-Zentrum Berlin für Materialien und Energie, Schwarzschildstr. 3, 12489 Berlin, Germany
[3] Helmholtz-Zentrum Berlin für Materialien und Energie, Young Investigator Group Hybrid Materials Formation and Upscaling, Kekuléstraße 5, 12489 Berlin, Germany

Received: 20 July 2022 / Received in final form: 14 November 2022 / Accepted: 2 February 2023

Abstract. To achieve a monolithic series interconnection of tandem solar cell devices consisting of a perovskite top cell and a CIGSe bottom cell, a two-terminal interconnection scheme is introduced that includes an additional, fourth patterning step, the so-called iso-cut, which separates the window layer stack between the two solar cells. The implementation of this interconnection scheme requires a process development for a total of four structuring steps, which was achieved by systematically varying the laser parameters. Based on a detailed characterization of the individual scribe line properties with respect to their scribe line depth, morphology, electrical functionality, chemical composition and their influence on adjacent and underlying layers, the optimal patterning parameters and suitable process windows were derived for each step, which is a prerequisite for a loss-free monolithic series interconnection in a tandem module.

Keywords: CIGSe / perovskite / tandem solar cells / laser / series interconnection / solar module / thin-film

1 Introduction

Within the last years, the power conversion efficiencies (PCE) for lab-scale metal-halide perovskite solar cells (PSCs) have been continuously improved [1] and recently reached efficiencies close to its theoretical limit. In order to overcome this limit and to utilize the irradiance of the sun more efficiently, an additional solar cell is typically used, which form together a tandem solar cell device. Tandem solar cells, composed of two in series interconnected individual solar cells stacked on top of each other are known as tandem devices in 2-terminal configuration. There, each sub-cell is optimized for the conversion of a specific range of the incoming sun light; the upper cell is more sensitive for the short-wavelength range whereas the lower cell is optimized for the longer-wavelength range. The tuning of the spectral sensitivity of each sub-cell depends on the utilized absorber material. For perovskite solar cells, as well as for copper-indium-gallium-diselenide (CIGSe) solar cells, the tuning of the bandgap energies over a broad range can be realized through compositional engineering. Thus, PSCs and CIGSe solar cells are suitable and complementary partners for tandem solar cell devices in 2-terminal configuration [2], whereby the perovskite cell is usually designed as a semi-transparent top cell [3]. On laboratory scale, two-terminal perovskite-CIGSe tandem solar cells have already been demonstrated with power conversion efficiencies approaching 25% [4]. The fabrication of tandem solar modules that go beyond the lab-scale tandem devices and have high power conversion efficiencies represents the next step for broad commercialization. For the fabrication of photovoltaic modules in such industrially relevant sizes, reliable patterning processes are required for the creation of monolithically series-interconnected perovskite top cells and CIGSe bottom cells.

Hence, the aim of this work is therefore to determine the optimal laser patterning parameters and to provide a guideline for the patterning of perovskite-CIGSe solar cells in order to enable monolithic series interconnection. This guideline is based on theoretical considerations that take into account material properties, ablation behavior, and electrical requirements to provide laser patterned scribe lines with optimal electrical functionality for monolithic series interconnection.

* e-mail: schultz@htw-berlin.de
[a] These authors contributed equally.

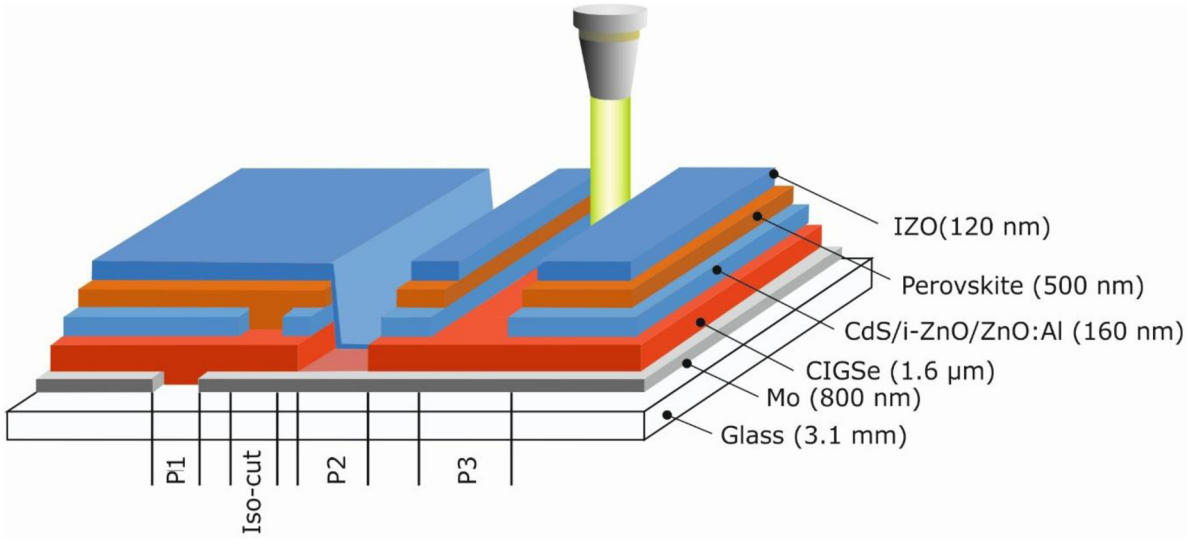

Fig. 1. Schematic cross-sectional representation of the perovskite-CIGSe layer stack with the respective materials and layer thicknesses. The adapted principle of monolithic series interconnection with four patterning steps (P1, iso-cut, P2, P3) adapted to tandem solar cells with a window layer stack is shown. The total width of all four lines including intermediate distances determines the interconnection width (dead area width).

In general, monolithic series-interconnections of single junction thin film solar cells is achieved by alternating layer deposition and patterning steps, typically referred to P1, P2, P3. The first (P1) and the last (P3) patterning steps electrically separate the front and back contact layers of neighboring cells, respectively. In contrast, the P2 patterning step removes the absorber layer locally to provide an electrical pathway from the back contact of one cell to the front contact of the adjacent cell. Thereby, the series interconnection is created. In two-terminal PSC/CIGSe tandem solar cells, the top PSC cell is interconnected in series with the CIGSe bottom cell via an intermediate window layer stack composed of CdS/i-ZnO/ZnO:Al. This intermediate window layer stack enables a more efficient charge carrier transport. However, it has to be separated by an additional scribe line, the iso-cut, to prevent the flow of photo-generated charge carriers from the bottom cell to the P2 scribe line. In earlier work, a novel interconnection scheme for such 2-terminal tandem devices comprising an iso-cut was developed (see Fig. 1) [5]. It can be seen that without this iso-cut, the top-cell would bypassed instead of interconnected in series with the bottom-cell. Thus, the iso-cut is patterned between the deposition of the window layer stack and the subsequent deposition of the top cell.

Pulsed lasers are the tool of choice for all these patterning tasks, as they allow layer-selective material removal with a high reproducibility at the same time. The general principles of laser patterning of thin-films, especially the laser-material interaction processes with a focus on laser-induced material modifications, have been investigated and described in detail in previous work [6–9]. In general, the success of laser scribing is based on precisely controlled energy input and is mainly dependent on the thicknesses, absorption behavior, and detailed configuration of the layer stack to be patterned. Consequently, optimal scribe lines are characterized by well-defined scribe line edges without unintended material modifications (i.e. due to excessively introduced laser energy) in their vicinity. The task of laser patterning of a specific scribe can be divided in two parts, one being the configuration of the patterning setup and the other being the determination of the resulting process window which includes suitable and promising patterning parameters. The configuration of the setup refers to the utilized laser, its wavelength and pulse duration as well as the chosen patterning approach (such as direct ablation, induced ablation, and induced direct ablation; cf. Fig. S1 [9]). Often, the configuration of the setup is already determined by the (optical) properties of the considered layer or layer stack. Once the configuration of the setup is established, the parameters forming the process window must be carefully considered to achieve the required scribe line properties such as width, depth, and smoothness of the scribe line bottom. In addition, the scribe line specific electrical requirements (i.e. high isolation resistance for the P1, iso-cut and P3; low series resistance for the P2) must be achieved. Since the change in laser energy per laser shot and the pulse-to-pulse overlap results in the cumulative energy input, the patterning process can be adapted to the specific requirements of the respective patterning steps. That is, for the P2 a clean and smooth scribe line bottom which is essential for low contact resistances, so a high pulse-to-pulse overlap is preferred. Otherwise, a rather low overlap is advantageous, as it minimizes the total energy introduced per laser spot area, which helps to avoid unintended material modifications.

In our study, for each scribe line required for monolithic series-interconnection of perovskite-CIGSe tandem solar cells, the listed points are discussed and clear conclusions are drawn. Moreover, several scribe lines are patterned with systematically varied fluence within the derived range of suitable fluences (process window). A characterization of

these scribe lines with regard to geometric properties, material-selective ablation, excess energy input, and an analysis of the composition of the residual material within the scribe lines is performed by laser-scanning microscopy (LSM), scanning-electron microscopy (SEM) with additional energy-dispersive X-ray spectroscopy (EDX) and electrical measurements. The electrical measurements were carried out line-by-line with a 2-point setup. This approach enables the direct determination of the electrical functionality of each scribed line without being influenced by the overall device performance and possible further losses. These investigations provide a comprehensive picture of the electrical, morphological, and compositional scribe line properties as a function of the laser fluence. From this, the conditions for an optimal process window and a high process reliability were derived. Following the same procedure as for the patterning of single perovskite solar cells explained in reference [10], we specify a range of suitable patterning parameters (process window) for the individual scribe lines as well as the selected fluence at which optimal scribe line behavior can be expected. The conclusive discussion of the question of how to pattern scribe lines with optimal properties also provides a guideline which applies even to different layer stacks.

2 Experimental

2.1 Sample preparation

The sample preparation processes followed the procedure for perovskite and CIGSe baseline samples described in detail elsewhere [7,11,12]. The monolithic tandem device layer-stack is prepared in substrate configuration on a glass substrate. A CIGSe cell is deposited on the glass and a perovskite cell is deposited on top. The CIGSe bottom-cell comprises a 800 nm Mo back contact, a CIGSe absorber layer of about 1600 nm, a 60 nm CdS buffer layer and a i-ZnO/ZnO:Al window layer stack of about 100 nm. The top cell consists of a perovskite absorber layer of approximately 500 nm composed of $Cs_{0.15}FA_{0.85}PbI_{2.55}Br_{0.45}$ sandwiched between a self-assembled monolayer (SAM) functioning as a hole-transmitting layer (HTL) and a C_{60} electron-transmitting layer as (ETL). Finally, an approximately 130 nm thick indium zinc oxide (IZO) layer is deposited as front contact.

2.2 Laser patterning

The sample patterning was carried out using a commercially available, customized laser system (Rofin Baasel Lasertech). This system is equipped with a nanosecond laser source (SL3PV) and a picosecond laser source (Time Bandwidth, Duetto). The ns laser emits laser pulses with a wavelength of 532 nm, its pulse durations is approximately 20 ns. A maximum pulse energy of about 32 µJ is emitted at 20 kHz. The ps laser emits laser pulses with a wavelength of 1064 nm or 532 nm, its pulse durations are approximately 10 ps and the maximum pulse energy of about 83 µJ is reached at 100 kHz for 1064 nm. The laser beam diameters in focal position were determined by applying the method of Liu [13], for the ns laser a diameter of 28.1 µm ± 10% and for the ps laser diameters of 40 µm ± 10% and 26.7 µm ±10% were determined for 1064 nm and 532 nm, respectively. The laser tool is equipped with fixed optics guiding the laser beam to the sample surface; whereas the sample translation is realized by a x-y motion system which enables velocities up to 1.2 m/s while at the same time, a positioning accuracy of about 5 µm for each stage is maintained. In order to avoid material degradation due to the ambient atmosphere and to collect dust and debris generated by the patterning process itself, the samples were patterned in a closed chamber with a continuous nitrogen flow and a window glass that allows the laser beams to pass through.

2.3 Characterization techniques

The scribe line geometry was examined using laser-scanning microscopy (Keyence VK-X260). This microscope illuminates the sample with a laser (408 nm). The installed planar achromatic objectives with a magnification of 10× to 150× allow a spatial image resolution of a few tens of nanometers. The specified accuracy in the vertical direction is in the range of few nanometers.

The electrical functionality of scribe lines was derived from resistance measurements that were repeated several times and statistically evaluated. The scribe line length is 10 mm, across this length the resistances for electrical isolation (P3) and the series resistance for interconnection (P2) were measured with contact needles in 2-point configuration. For all electrical measurements, piercing through the layer stack by the contact needles was prevented by an adhesive copper tape in between which also improves the electrical contact resistance. The vertical edges of the test patches separated by the laser were scratched manually using a diamond-tip needle.

The morphology of the laser scribed lines was also examined by scanning-electron microscopy (SEM, Hitachi S4100). This instrument is equipped with a detector for energy-dispersive X-ray spectroscopy (EDX), which allows an analysis of the composition of the material within the scribed lines and their vicinities. The analyses of the composition of the scribe line trenches aim to reveal compositional material alterations in this area. For this purpose, the corresponding scribe lines and their vicinities where excited by an electron beam and the corresponding element-selective mappings were recorded. We used an accelerating voltage of 10 kV. For this, the excitation depth is in the range of about 0.8 µm to 1 µm, which is suitable for the respective layer thicknesses; the spatial resolution is approximately 0.5 µm [14]. For data evaluation, three profiles across each scribe line were extracted from the images, containing the elemental counts as a function of the xy-position. Subsequently, these profiles were smoothed (moving average) and normalized. Accordingly, the elemental count of an undisturbed remote area is 1. Higher or lower values correspond to lower layer exposure and layer removal, respectively.

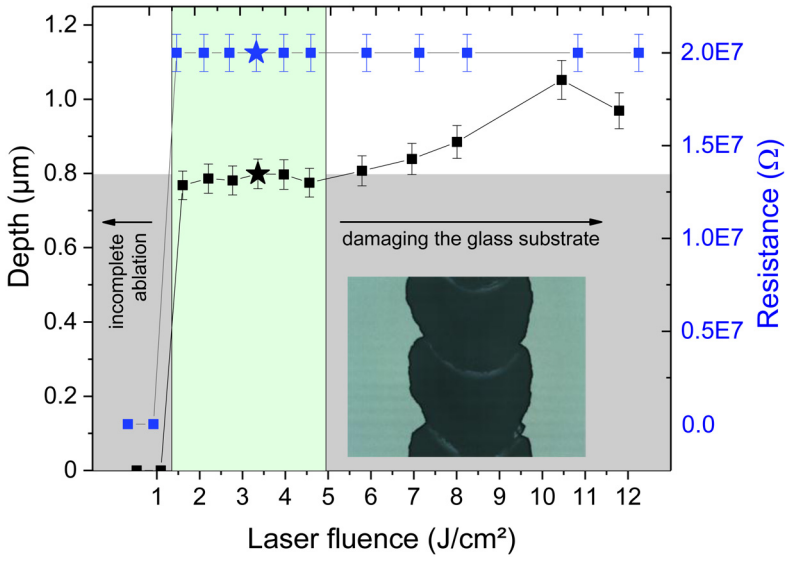

Fig. 2. P1 scribe line depth (left y-axis, black squares) and electrical resistance across the scribe line (right y-axis, blue squares) as a function of the applied laser fluence. The range of suitable fluences is marked by the light green area, the selected fluence with an asterisk. The gray area illustrates the Mo back contact.

3 Results and discussion

3.1 Setup configuration and scribe line essentials

The first step is to determine the configuration of laser patterning setup. In the case of our perovskite-CIGSe tandem solar cells a Mo-coated glass substrate is used onto which the subsequent layers were deposited. The opaqueness of the Mo layer restricts patterning of the subsequent layers through the glass substrate (i.e. by induced ablation, cf. Fig. S1B), except for the P1 scribe line itself.

When selecting the most suitable laser pulse duration, the thermal sensitivity of the material under investigation must be considered [7]. For perovskite-CIGSe tandem solar cells, a ps laser is in principle well suited, as the CIGSe has a strong thermal sensitivity of [15]. It is assumed that ps laser pulses enable almost athermal ablation due to their short pulse lengths. However, ns laser pulses are well-suited for P2 patterning as they enable the conversion of the CIGSe absorber material into a conductive, Cu-rich phase [16,17]. Unintended material alterations can always be caused by improper patterning parameters [9]. The selection of the wavelength applied for patterning depends strongly on the optical properties, especially the absorption coefficient, of the individual layers of the stack to be processed (cf. Fig. S2). It has been found that the use of a wavelength of 532 nm is advantageous since the front contact layer as well as the intermediate layer is transparent to this wavelength and enables induced direct material ablation [15] (cf. Fig. S1C). As a result, the patterning can be carried out with minimal laser energy. Moreover, this wavelength can typically be provided by solid state laser, which are widely used. For P1 patterning of the Mo layer, it is expected that the application of 1064 nm and of 532 nm laser pulses will not lead to significant differences in the ablation behavior due to the broad band absorption behavior.

The scribe line width required for the specific electrical functionality affects the configuration of the patterning setup in terms of laser beam diameter and optical lenses and generally depends on the considered layer stack or on the material that subsequently fills the scribe line. A detailed study of the electrical losses for monolithic series interconnections is given by Brecl et al. [18] for a single junction CIGSe solar module. In order to approximate the required scribe line widths based on this study, several assumptions have to be made about the material properties with respect to the electronic constants. Typically, these considerations result in widths in the range of about 20 µm, either to provide low-ohmic contacts for P2 patterning or to create scribe lines with sufficiently large resistances as required for P1, iso-cut, and P3 patterning. Advantageously, it has been shown that these scribe line widths can be achieved by commercially available optical components with reasonable effort.

3.1.1 P1 patterning

The P1 scribe line is intended to electrically separate neighboring cells or regions, at the same time the widths of the cells are determined. The P1 patterning process has been investigated by several groups who analyzed the ablation behavior of differently deposited Mo layers on glass substrates [19–21]. It was shown that by applying glass-side patterning (cf. Fig. S1B) with rather low pulse-to-pulse overlap, a beneficial ablation behavior in terms of scribe line quality (rims, width, glass damage, etc.) can be achieved by making use of the internal strain of the Mo layer [22–24]. A systematic variation of the laser fluence and the corresponding measured scribe line depth and electrical resistance across the scribe line is shown in Figure 2. The applied pulse-to-pulse overlap is about 15% (see Tab. 1 for a complete list of the laser parameters used). It can be observed that at fluences of about 1.5 J/cm^2 the

Table 1. Experimentally determined optimal parameters used for laser patterning.

		Unit	P1	Iso-cut	P2	P3
Patterning regime (cf. Fig. S1)			Induced ablation	Induced direct ablation	Direct ablation	Induced direct ablation
Pulse duration	τ_P	s	$\approx 10^{-11}$	$\approx 10^{-11}$	$\approx 10^{-9}$	$\approx 10^{-11}$
Wavelength	λ	nm	1064	532	532	532
Pulse-to-Pulse overlap		%	≈15	≈25	≈65	≈35
Laser fluence	F	J/cm^2	3.36	0.53	9.38	3.16

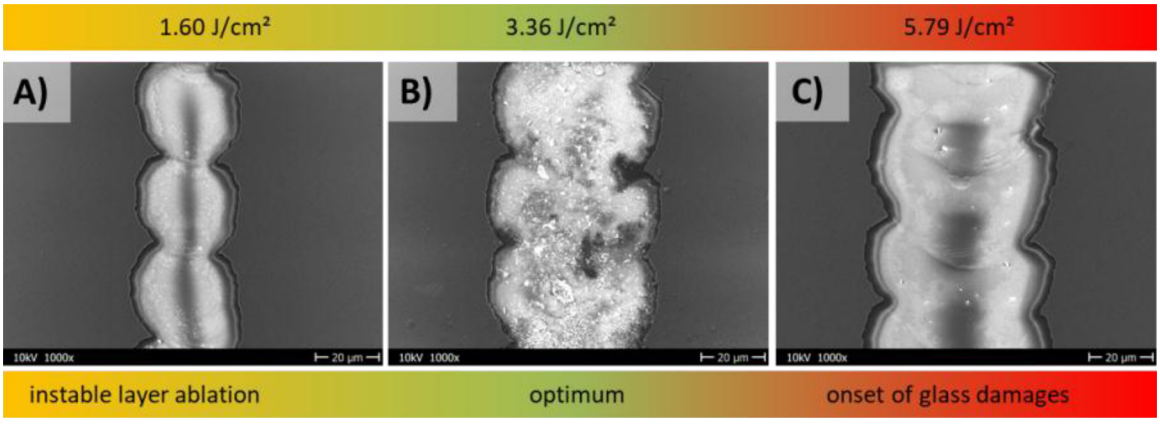

Fig. 3. Comparison of SEM images of P1 scribe lines patterned with three characteristic fluences: (A) 1.16 J/cm^2 (incomplete layer ablation), (B) 3.36 J/cm^2 (optimal scribe line properties), and (C) 5.79 J/cm^2 (onset of glass damages). The color bars indicate the respective patterning regimes and the chosen patterning fluences. The magnification the images is 1000×, the excitation voltage is 10 kV.

ablation of the Mo layer starts, but still leads to (partially) incomplete ablation. At higher fluences of about 3.36 J/cm^2 the required scribe line depth of 800 nm is achieved continuously, indicating the reliable ablation of the complete Mo layer. At fluences up to 5 J/cm^2, the scribe line depth remains constant; with increasing fluence the scribe line depth slowly increases again. This observation is attributed to the explosive ablation of the Mo after a certain amount of energy was introduced and the tensile strength of the Mo layer is exceeded. Below this threshold of about 1 J/cm^2 the deposited energy creates only cracks in the Mo layer and is not high enough to remove the layer. With increasing fluence the ablation of the Mo starts abruptly until the underlying glass substrate is damaged by the excessive energy input, which can be seen by the increasing scribe line depth from about 5 J/cm^2.

Corresponding to the step-like increase of the scribe depth, the measured electrical resistance increases from its sheet resistance (well below 1 Ω/□) to about 20 MΩ which refers to the highest resistance that could be measured with the measuring device used. Based on these observations, a suitable range of patterning parameters is found between 1.5 J/cm^2 and 5 J/cm^2 as shown in Figure 2. There, the light green area refers to the range of suitable patterning parameters. A direct comparison of SEM images of representative surfaces aside the laser scribe lines is shown in Figure 3. These scribe lines are patterned closely above the ablation threshold (A), with the selected fluence (B), and with excessive energy input at too high fluence (C). The SEM images show that too low fluence results in instable scribe line widths, while excessive energy input causes damages of the underlying glass substrate. At the selected fluence, reliable scribe line patterning is characterized by homogeneous lines with a well reproducible line widths and edges without rims or cracks. Thus, it is considered as optimum, as it can be deduced from Figure 2 and Figure 3. The optimal fluence for P1 patterning is about 3.36 J/cm^2, which is sufficiently far away from both, incomplete layer ablation (<1.5 J/cm^2) and the onset of glass damage (>5 J/cm^2).

3.1.2 Iso-cut patterning

After patterning the Mo back contact and depositing the CIGSe absorber including the CdS/i-ZnO/ZnO:Al window layer stack, the patterning of the latter is carried out to prevent bypassing the top-cell. In contrast to P1 patterning of the sole Mo layer, the heat-sensitive CIGSe absorber is located underneath the window layer stack. Thus, iso-cut patterning is the most crucial step. As discussed earlier, the CIGSe absorber layer is very sensitive to thermal influences [7,25]. Thus, in order to avoid unintended material

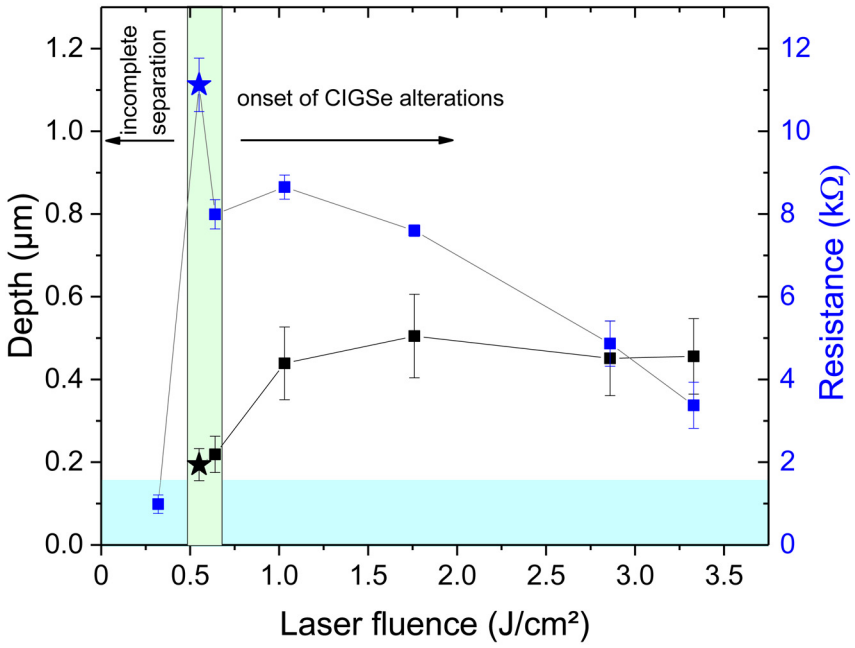

Fig. 4. Iso-cut scribe line depth (right y-axis, black squares) and electrical resistance across the scribe line (left *y*-axis, blue squares) as a function of the applied laser fluence. The range of suitable fluences is marked by the light green area, the selected fluence with an asterisk. The cyan area illustrates the intermediate CdS/i-ZnO/ZnO:Al window layer stack.

alterations, the patterning should be carried out with carefully adjusted fluence and low pulse-to-pulse overlap. Thus, for the determination of the optimal patterning parameters, a pulse-to-pulse overlap of about 25% was applied while the laser fluence was systematically varied (see Tab. 1 for a complete list of the laser parameters used). In Figure 4, the resulting scribe line depth and electrical resistance across the corresponding scribe line as a function of the applied laser fluence are shown.

There, it can be observed that the measured scribe line depth rises immediately to the thickness of the window layer stack and increases continuously up to a fluence of about slightly below $2\,\mathrm{J/cm^2}$. At higher fluence, the scribe line depth saturates or even decreases again. A similar trend can also be observed for the measured resistances across the scribe line. There, the highest resistance was measured for the lowest fluence that still results in the ablation of the window layer stack. With increasing fluence, the measured resistance decreases from its maximum of about 11 kΩ down to about 3 kΩ at about $3.5\,\mathrm{J/cm^2}$. It is assumed that this behavior is related to the alteration of the CIGSe absorber, which is increasingly modified at higher fluences, while the application of low fluences prevents these alterations and only leads to induced direct material ablation of the window layer stack. Moreover, these results indicate a rather narrow window of suitable fluences (indicated by the light green area in Fig. 4) in which optimal scribe line properties can be achieved.

In Figure 5 SEM images of scribe lines patterned at the ablation threshold (A), at the selected fluence (B), and with excessive fluence (C) are shown. These images clearly show that the scribed line at the ablation threshold incomplete separates the window layer stack (A) and that the application of excessive fluence (C) induces material alterations of the CIGSe, as indicated by the scribe line bottom, which has a solidified appearance compared to the sharp structures of the CIGSe when patterned at selected fluence (or even lower).

In order to understand this observation, a compositional analysis was carried out by EDX spectroscopy. Figure 6 shows the evaluation of the material composition of laser scribed lines and their vicinities as a function of the applied fluence. There, the left *y*-axis depicts the course of the normalized relative amount of Zn (L line) and the right *y*-axis correspondingly the course of elemental copper (L line), which belong to the window layer stack and the CIGSe absorber, respectively, whereby the value 1 refers in each case to the area untreated by the laser. The corresponding data points were extracted from the EDX mappings of the individual elements (examples can be found in Fig. S3). The datapoint marked with an asterisk is assigned to the previously derived selected fluence for optimal patterning. The graphs in Figure 6 show, that the application of even very low fluences (below $0.5\,\mathrm{J/cm^2}$) results in an immediate drop of the Zn signal (left y-axis), while for higher fluences the signal remains at a very low constant level. At the same time, the Cu signal rapidly rises remaining also at an almost constant level for moderate fluences, while it increases slightly at higher fluences (above $3\,\mathrm{J/cm^2}$). Correspondingly, by comparing these curves with the SEM images shown in Figure 5, the strong decrease of the Zn signal clearly indicates the removal of the window layer stack and the rising Cu signal can be assigned to the exposed CIGSe absorber. It is assumed, that the increase of the Cu signal at higher fluences is

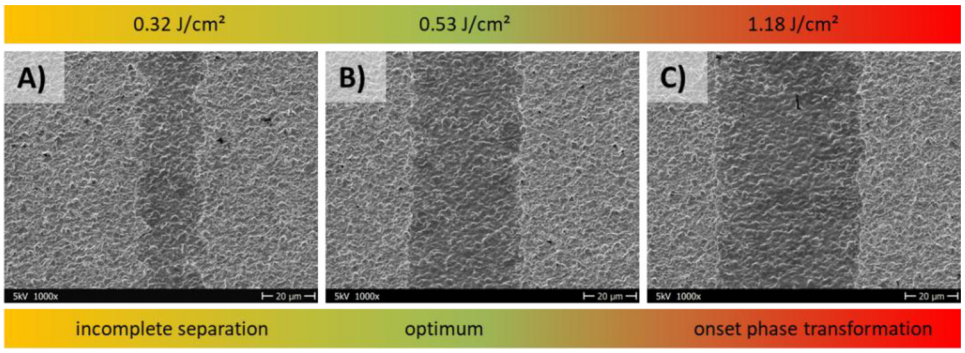

Fig. 5. Comparison of SEM images of iso-cut scribe lines patterned with three characteristic fluences: (A) $0.28\,\mathrm{J/cm^2}$ (incomplete separation), (B) $0.53\,\mathrm{J/cm^2}$ (optimal scribe line properties), and (C) $1.18\,\mathrm{J/cm^2}$ (onset of transforming the CIGSe absorber into a conductive phase). The color bars indicate the respective patterning regimes and the chosen patterning fluences. The magnification of the images is 1000×, the excitation voltage is 10 kV.

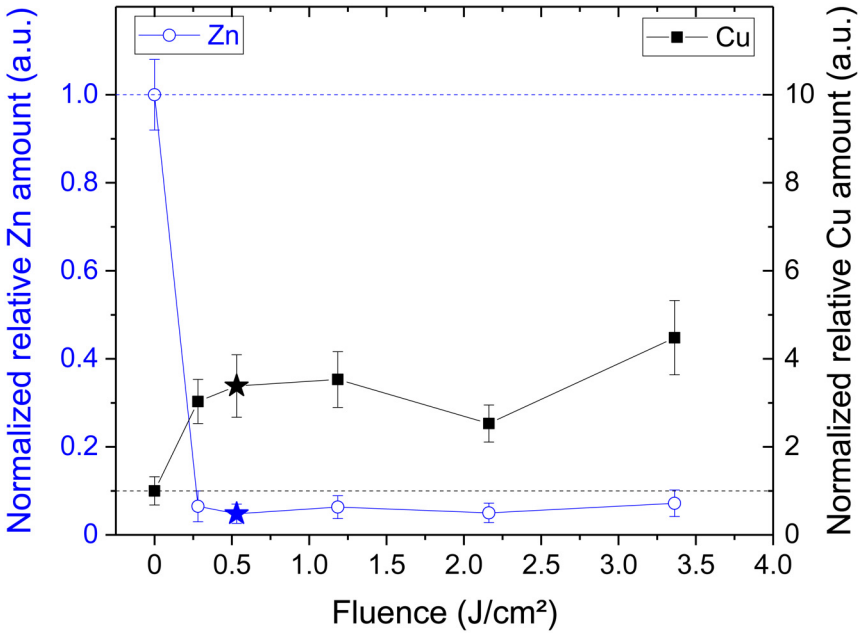

Fig. 6. EDX investigation of the material composition in the iso-cut scribe lines as a function of the applied laser fluence. The blue open circles are assigned to elemental Zn (L line), which is an indicator for the window layer stack (left y-axis). The black squares refer to elemental Cu (L line), which represents the underlying CIGSe absorber (right y-axis). The selected fluence is marked with an asterisk.

related to the phase transformation of CIGSe, which shows the evaporation of Ga and In while Cu-rich material remains in the trench [16,26].

The observed behavior suggests that the window layer stack can be selectively ablated with a fluence ($\sim 0.53\,\mathrm{J/cm^2}$) which is slightly above the ablation threshold. Applying this fluence enables the complete removal of the window layer stack without substantial compositional alterations within the underlying absorber layer, thus it is considered the optimal fluence. The application of higher fluences still results in the ablation of the window layer stack, but in parallel, the transformation of the CIGSe into a conductive phase also sets in, which agrees well with the measured resistance and the observed solidified appearance of the CIGSe within the iso-cut scribe line.

3.1.3 P2 patterning

In contrast to P1 and iso-cut patterning aiming to electrically separate the respective layers, the objective of the P2 scribe is to provide a low-ohmic contact between the back and front contact layer via opening the absorber layers. In order to achieve a low ohmic contact between the front and the back contact, typically, the complete removal of the absorber layer is required. The P2 patterning step is a balancing act between complete material removal and the avoidance of damages to the underlying contact layer (i.e. deterioration of the sheet resistance). In accordance to Ohm's law, wider scribe lines provide lower contact resistances, which can be achieved by a high pulse-to-pulse overlap which often also results in a clean and smooth scribe line bottom for this perovskite-CIGSe layer configuration.

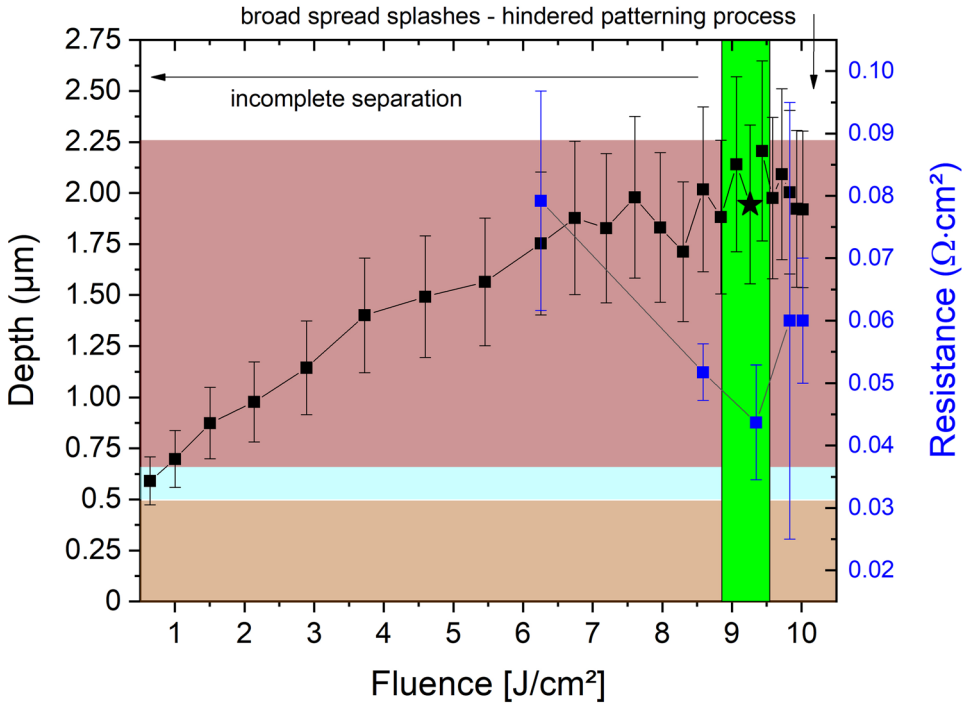

Fig. 7. P2 scribe line depth (right y-axis, black squares) and electrical resistance across the scribe line (left y-axis, blue squares) as a function of the applied laser fluence. The range of suitable fluences is marked by the light green area, the selected fluence with an asterisk. The brownish area illustrates the perovskite layer, the cyan area refers to the window layer stack, and the dark red area refers to the CIGSe absorber layer.

A special feature of CIGSe solar cells is that the P2 patterning can be carried out by transforming the CIGSe into a conductive phase instead of removing the entire absorber material down to the Mo back contact. This approach is based on the direct ablation process (cf. Fig. S1A) and was initially presented by Westin et al. [27]. Subsequently, we further elaborated this approach and showed that the phase transformation of the CIGSe for P2 patterning results in electrical properties which are comparable to the standard P2 approach [16]. Thus, for P2 patterning of perovskite-CIGSe solar cells, the phase transformation process for P2 patterning appears to be beneficial compared to the material removal process, as it provides similarly low contact resistances while reducing the risk of damaging the underlying Mo layer.

In order to obtain the optimal fluence for this approach based on phase transformation, the laser fluence for P2 patterning was systematically varied while the pulse-to-pulse overlap was about 65% (see Tab. 1 for a complete list of the laser parameters used). In Figure 7, the measured scribe line depth and the corresponding series resistance down to the Mo as a function of the applied fluence are shown. There, it can be observed that the measured scribe line depth continuously increases with increasing fluence and slowly saturates at about 9 J/cm^2. Moreover, it can be seen that already below 1 J/cm^2 the perovskite absorber is completely removed, followed by the removal of the intermediate window layer stack up to the almost complete removal of the CIGSe absorber layer at about 10 J/cm^2, leaving highly conductive Cu-rich residual material within the scribe line [16,27]. The application of higher fluences (within the range of available fluences of up to 10 J/cm^2) does not lead to deeper scribe lines. On the contrary, the scribe line depths decrease slightly which is attributed to the fact that molten absorber material "refills" the scribe line. The series resistance of the P2 scribe line was measured after deposition of the IZO layer. Here, an opposite trend compared to the scribe line depth can be observed. With increasing fluence, the series resistance decreases continuously from about 235 $\Omega \cdot$cm^2 (reference, without scribe line) to 0.04 $\Omega \cdot$cm^2 for a fluence of about 9.4 J/cm^2. At higher fluences the measured series resistances remains almost constant at this very low level.

Consequently, within the range of suitable fluence represented by the light green area in Figure 7, optimal scribe lines are achieved at a fluence of about 9.4 J/cm^2, which are characterized by geometrically well-defined scribe lines and solidified, phase transformed residual material at the scribe lines bottom, providing a low ohmic series resistance to the Mo back contact [16,26]. In Figure 8 the SEM images of scribe lines patterned with insufficient fluence (A), selected fluence (B), and too high fluence (C) are shown. There, it can be observed that insufficient fluence results in incomplete transformation of the CIGSe absorber, as is indicated by the shallow scribe line. In contrast, excessive fluence results in melting and boiling of the material which forces the formation of splashes which were found in a wide area next to the lines [8]. Moreover, the formation of splashes clearly indicates excessive input of laser fluence which also causes melting of the scribe line

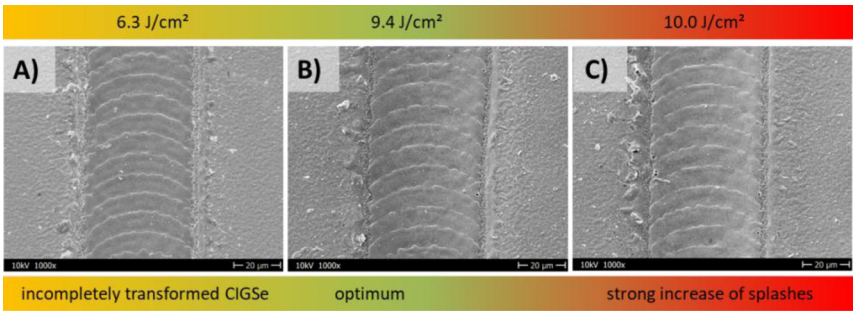

Fig. 8. Comparison of SEM images of P2 scribe lines patterned with three characteristic fluences: (A) 6.3 J/cm^2 (incompletely transformed CIGSe), (B) 9.4 J/cm^2 (optimal scribe line properties), and (C) 10.0 J/cm^2 (strong formation of splashes). The color bars indicate the respective patterning regimes and the chosen patterning fluences. The magnification of the images is 1000×, the excitation voltage is 10 kV.

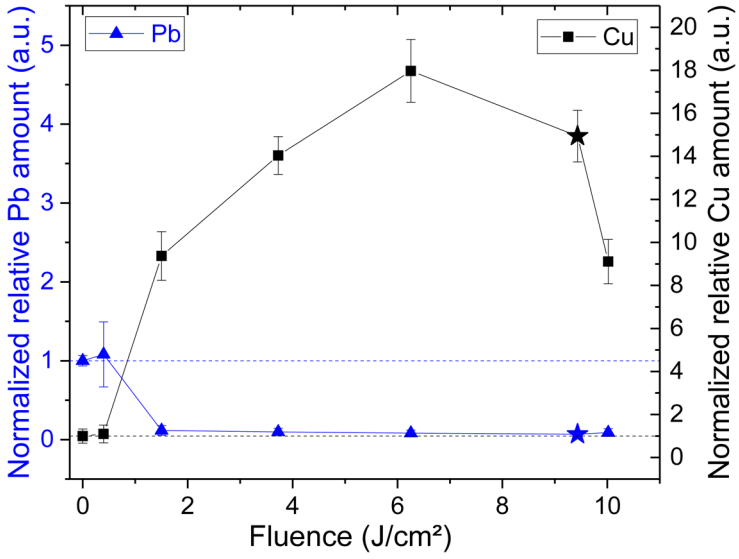

Fig. 9. EDX investigation of the material composition in the P2 scribe lines as a function of the applied laser fluence. The blue triangles correspond to elemental Pb (M line) used as indicator for the perovskite absorber (left y-axis). The black squares refer to elemental Cu (L line), which corresponds to the underlying CIGSe absorber (right y-axis). The selected fluence is marked with an asterisk.

edges. This molten material might partially flow from the scribe line edges towards the scribe center reducing the scribe line depth. This case is shown in Figure 8B, where the scribe line depth comprises almost the entire depth of both absorbers, indicating the complete removal of the perovskite layer and the window layer stack, while the strong thermal treatment initiates the phase transformation of the CIGSe absorber layer. The latter is essential to transform the CIGSe into a conductive phase for a low-ohmic series interconnection.

The changes in the elemental composition of the material within the scribe line as a function of the laser fluence are shown by Figure 9 for selected scribe lines. In this figure, the normalized elemental amounts of Pb (M line) and Cu (L line) are shown, indicating the perovskite and the underlying CIGSe absorber, respectively. It can be seen that the Pb content immediately decreases after the laser treatment and remains at constant low level for fluences above 2 J/cm^2. At the same time, the Cu signal rises continuously, reaches its maximum at about 6 J/cm^2 and decreases thereafter. The application of higher fluences does not affect the Pb signal, but the Cu signal drops rapidly. The course of the Pb signal indicates that the entire perovskite absorber is removed at a fluence of about 2 J/cm^2, while higher fluences are needed to completely phase transform and partially remove the CIGSe absorber. Considering the corresponding SEM images, the course of the Cu signal can be interpreted as follows: For low fluences (below 2 J/cm^2) the perovskite layer is continuously ablated exposing the CIGSe underneath. Obviously, the highest Cu signal is achieved at about 6 J/cm^2 which might be explained by already strongly phase-transformed CIGSe without massive ablation of the absorber layer (cf. Fig. 8A, shallow trench). As a result, the detected amount of Cu is highest with respect to the excitation volume comprising almost the entire CIGSe layer, while at higher fluences (beyond 6 J/cm^2) the ablation of the CIGSe leads to a continuous decrease of the excitation volume and thus to a decreasing Cu signal.

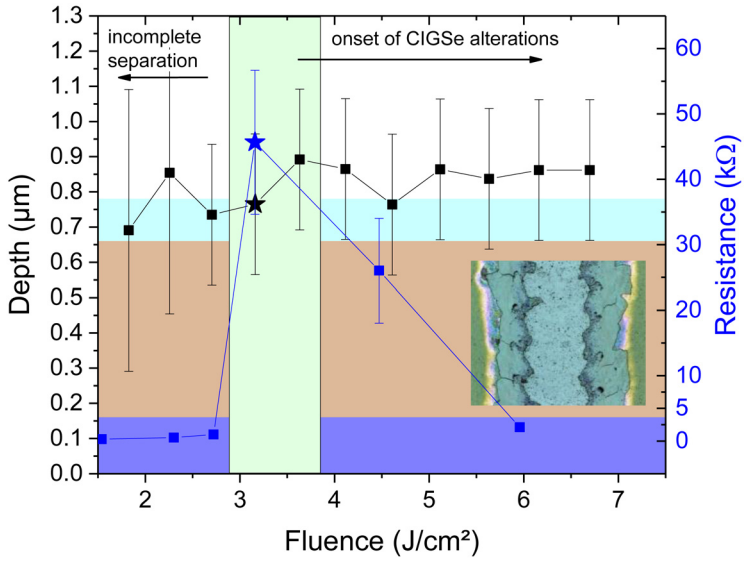

Fig. 10. P3 scribe line depth (right y-axis, black squares) and electrical resistance across the scribe line (left y-axis, blue squares) as a function of the applied laser fluence. The range of suitable fluences is marked by the light green area, the selected fluence with an asterisk. The blue area corresponds to the IZO front contact, the brownish area refers to the perovskite layer, and the cyan area depicts the window layer stack.

Thus, the optimal scribe line properties are found at the selected laser fluence for P2 patterning of about 9.4 J/cm^2. There, the perovskite absorber layer as well as the intermediate window layer stack are reliably ablated and the CIGSe absorber is completely transformed into a conductive phase remaining as residual material in the scribe line.

3.1.4 P3 patterning

The P3 scribe line is also intended to electrically separate neighboring cells, thus its properties should also be similar to the previously discussed P1 scribe line and the iso-cut. In previous studies, the P3 patterning process for CIS and CIGSe solar cells has been already investigated [15,28]. It has been shown that for successful P3 patterning in terms of the resulting electrical functionality of the solar cell, the CIGSe absorber layer including the window layer stack does not necessarily have to be completely removed. A P3 patterning approach, which easily causes compositional changes in the scribe line vicinity [25] is assumed to lead to enhanced charge carrier trapping [7]. In contrast, due to the thermal sensitivity of the CIGSe, it is beneficial to selectively ablate only the window layer stack, thus avoiding laser-induced material alterations.

Due to the possibility of performing an induced direct material ablation process, significantly lower laser fluences are required, preventing compositional alterations in the vicinity of the P3 scribe lines. In contrast, for P3 patterning of perovskite solar cells, it was elaborated that the thermal impact during the patterning step does not negatively affect the electrical functionality. Thus, a complete removal of the front contact layer and the underlying perovskite absorber is common [10]. It is advantageous to adapt this approach to the current case of P3 patterning of our perovskite-CIGSe tandem devices. In this case, the patterning of the P3 scribe line includes the removal of the IZO front contact, the perovskite absorber, and the selective ablation of only the underlying window layer stack.

For all these scribe lines a rather low pulse-to-pulse overlap is beneficial since it prevents excessive energy input into the surrounding material while only a continuous separation must be ensured. As discussed earlier, a rather low pulse-to-pulse overlap should be preferred to prevent these material alterations. In our study, an overlap of about 35% was applied for P3 pattering while the laser fluence was systematically varied (see Tab. 1 for a complete list of the laser parameters used). In Figure 10, the resulting scribe line depths and the corresponding resistance across the scribe line as a function of the applied fluences are shown; the range of suitable fluences is marked by the light green area, the selected fluence is marked with an asterisk. There, it can be seen that even the lowest applied fluence creates almost the desired scribe line depth. With increasing fluence the scribe line depths increase slightly to reach a rather stable level corresponding to the total thickness of the front contact, the perovskite, and the window layer stack. The large error bars, especially for fluences below 2.5 J/cm^2, result from the averaging of several adjacent profile measurements with partially strongly fluctuating scribe line depths. At the same time, the corresponding resistances measured across the scribe line clearly show a maximum value of about 50 kΩ at a fluence of about 3.16 J/cm^2. Below and above this fluence the resistance rapidly drops. An indication of the behavior is given by Figure 11 showing SEM images of representative scribe lines. For the cases of too low applied laser fluence (Fig. 11A) the incomplete removal of the window layer stack leaves "bridges" enabling no proper electrical separation. In contrast, the application of excessive fluence (Fig. 11C) reliably removes these "bridges" but alterations

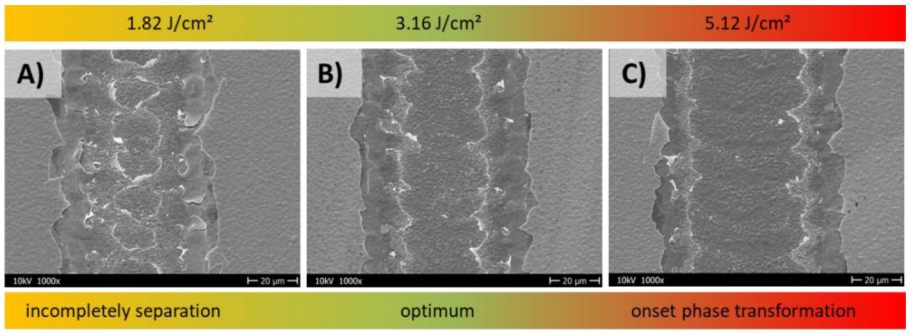

Fig. 11. Comparison of SEM images of P3 scribe lines, patterned with (A) 1.82 J/cm^2, (B) 3.16 J/cm^2, (C) and 5.12 J/cm^2 resulting in incomplete separation, optimal scribe line properties, and the onset of phase transformation of the underlying CIGSe absorber layer, respectively. The color bars above and below mark the optimal fluences for patterning and summarize the substantial findings, respectively. The magnification the images is 1000×, the excitation voltage is 10 kV.

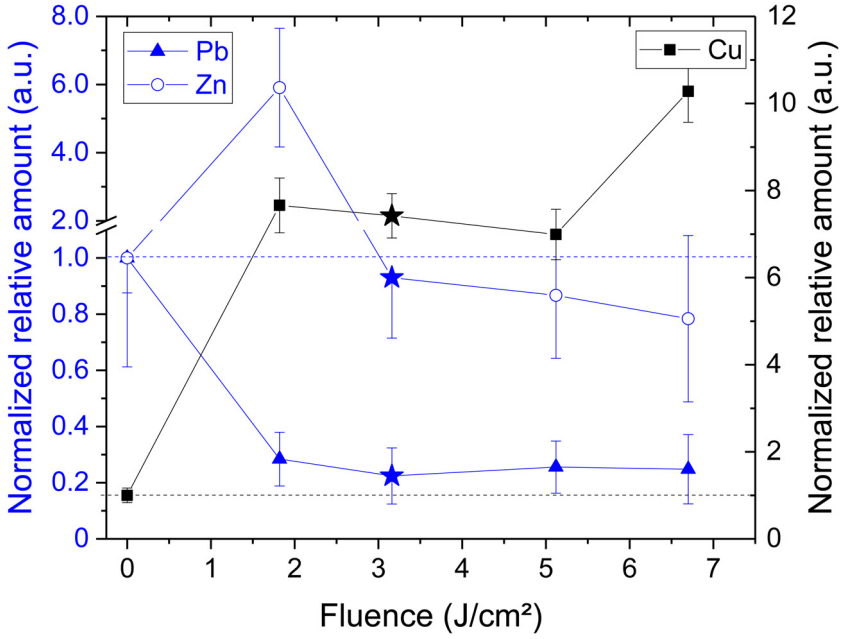

Fig. 12. EDX investigation of the material composition in the P3 scribe lines as a function of the applied laser fluence. The blue triangles represent elemental Pb (M line) and the blue open circles represent elemental Zn (L line), which are indicators for the perovskite absorber and the intermediate window layer stack, respectively. The elemental Cu (L line) signal is represented by black squares and is used as an indicator for the CIGSe absorber (right y axis). The selected fluence is marked with an asterisk.

of the CIGSe absorber set in, as indicated by a partially solidified surface of the scribe line bottom: as a result, a proper electrical separation across the scribe line is prevented. The selected fluence (Fig. 11B), on the other hand, is sufficiently high to reliably create the required scribe line depth. In addition, there is sufficient electrical separation, as this fluence is still below the onset of laser-induced alterations of the CIGSe (indicated by the absence of solidified areas at the scribe line bottom).

To investigate the elemental compositions of the material in the scribe line vicinity, the elemental counts of Pb (M line), Zn (L line), and Cu (L line) were utilized to identify the perovskite, the intermediate window layer stack, and the CIGSe absorber, respectively. The behavior of the elemental counts as a function of the applied fluence is shown in Figure 12. There it can be seen that with increasing fluence, the Zn signal and the Cu signal rise, while the Pb signal drops. With further increasing fluence the Pb signal slightly decreases to a constant value. In contrast, the Zn signal drops rapidly whereas the Cu signal remains constant and rises again at about 7 J/cm^2. This behavior indicates the immediate removal of the perovskite, exposing the underlying window layer stack. A further increase of the laser fluence causes the ablation of the window layer stack at about 3 J/cm^2, with the Cu signal remaining at a rather constant level. Only at higher fluences (about 6 J/cm^2) the Cu signal increases further. This behavior clearly indicates an optimal behavior of the scribe line properties at the selected fluence for P3 patterning of about 3.16 J/cm^2, which is marked with an asterisk. There, the results clearly show the complete removal of the front contact, the perovskite, and the

window layer stack exposing the CIGSe absorber, but remaining unchanged in the region of the optimal fluence. Beyond this optimal fluence, the CIGSe absorber becomes continuously phase transformed, resulting in a strong increase of the Cu signal.

Thus, when using fluences below 2.5 J/cm^2, patterning results in incomplete layer separation whereas higher fluences produce sufficiently deep scribe lines but also promote laser-induced material alterations (cf. Fig. 11). At a fluence of around 3.16 J/cm^2 both, reliable material ablation with sufficient laser separation and the avoidance of unintended material alterations are possible (for a summary of the laser parameters see Tab. 1).

4 Summary

The laser-based patterning of perovskite-CIGSe tandem solar cells for monolithic series interconnection has been investigated. In a first step, the configuration of the laser patterning setup was derived. The application of ps pulses enables the removal of the thin window layer stack (iso-cut and P3) while avoiding unintended thermal effects. In contrast, the use of ns pulses for P2 patterning, appears advantageous at present. But due to the strong thermal sensitivity of the CIGSe, it can be assumed that similarly good results can be achieved with ps laser pulses as already shown on single junction CIGSe solar cells [17,29].

The wavelength of 532 nm enables material selective material by induced ablation, further decreasing the fluence required for material removal and consequently reducing the risk of unintended material alteration. Based on these considerations, the laser fluence was systematically varied for each scribe line and analyzed by laser-scanning microscopy and EDX spectroscopy to characterize the scribe line depth and width and the material composition within the scribe line, respectively. Resistance measurements were also taken across all scribe lines to verify their electrical functionality. By using this approach, optimal process windows were determined for each scribe line. Moreover, the results clearly show that by carefully considering the material properties in terms of their behavior during laser patterning, the configuration of the patterning setup can be derived, which enables a straight-forward approach to define process windows and to approximate optimal patterning parameters even without electrical measurements of the solar cell. In a next step, the determined optimal patterning parameters will be applied for the production of a complete device in order to prove the series interconnection in a tandem module on the basis of the j-V characteristic curve.

Conflict of interests

The authors declare no conflicts of interests.

This work was supported by the HTW Berlin (project "LasTa"). The authors J.D. and E.U. gratefully acknowledge funding from the German Ministry of Education and Research (BMBF) for the Young Investigator Group Hybrid Materials Formation and Scaling (HyPerFORME) within the program "NanoMatFutur" (grant no. 03XP0091) and the "SNaPSHoTs"project (grantno. 01IO1806). Moreover, the authors acknowledge experimental support of the PVcomB and the HZB (EE-IS) teams, especially Carola Klimm for SEM and EDX measurements.

Author contribution statement

Christof Schultz: Investigation, Data curation, Visualization, Validation, Writing – Original Draft, Writing – review & editing. Guillermo Antonio Farias Basulto: Investigation, Data curation, Resources. Nicolas Otto: Investigation, Formal analysis, Data curation. Janardan Dagar: Methodology, Resources. Andreas Bartelt: Validation. Rutger Schlatmann: Resources, Supervision. Eva Unger: Methodology, Resources, Supervision. Bert Stegemann: Conceptualization, Visualization, Writing – original draft, Writing – review & editing, Supervision.

Supplementary material

Figure S1: Direct ablation (A), induced ablation (B), and induced direct ablation (C) for an absorbing layer on a transparent glass substrate (A, B) and a transparent layer on a glass substrate (C) irradiated by a laser beam.

Figure S2: Comparison of the absorption coefficients of the specific layers used in the perovskite-CIGSe tandem solar cell.

Figure S3: EDX mappings of the P2 lines, patterned with (A) 6.3 J/cm² (too low fluence), (B) 9.4 J/cm² (optimum fluence), (C) 10.0 J/cm² (too high fluence). Shown are the relative amounts of elemental Cu and Pb as the main absorber constituents of both solar cell absorbers. The excitation voltage is 10 kV for all images.

The Supplementary Material is available at https://www.epjpv.org/10.1051/epjpv/2023007/olm.

References

1. M.A. Green, E.D. Dunlop, J. Hohl-Ebinger, M. Yoshita, N. Kopidakis, K. Bothe, D. Hinken, M. Rauer, X. Hao, Solar cell efficiency tables (Version 60), Progr. Photovolt.: Res. Appl. **30**, 687 (2022)
2. M. Jošt, T. Bertram, D. Koushik, J.A. Marquez, M.A. Verheijen, M.D. Heinemann, E. Köhnen, A. Al-Ashouri, S. Braunger, F. Lang, B. Rech, T. Unold, M. Creatore, I. Lauermann, C.A. Kaufmann, R. Schlatmann, S. Albrecht, 21.6%-efficient monolithic perovskite/Cu(In,Ga)Se2 tandem solar cells with thin conformal hole transport layers for integration on rough bottom cell surfaces, ACS Energy Lett. **4**, 583 (2019)
3. M. Nakamura, C.C. Lin, C. Nishiyama, K. Tada, T. Bessho, H. Segawa, Semi-transparent Perovskite Solar Cells for Four-Terminal Perovskite/CIGS Tandem Solar Cells, ACS Appl. Energy Mater. **5**, 8103 (2022)
4. M.A. Ruiz-Preciado, F. Gota, P. Fassl, I.M. Hossain, R. Singh, F. Laufer, F. Schackmar, T. Feeney, A. Farag, I. Allegro, H. Hu, S. Gharibzadeh, B.A. Nejand, V.S. Gevaerts, M. Simor, P.J. Bolt, U.W. Paetzold, Monolithic two-terminal perovskite/CIS tandem solar cells with efficiency approaching 25%, ACS Energy Lett. **7**, 2273 (2022)

5. C. Schultz, G. Farias-Basulto, D. Schmidt, M. Fenske, J. Dagar, A. Bartelt, R. Schlatmann, E. Unger, B. Stegemann, Series interconnection of monolithic 2-terminal CIGSe-perovskite tandem cells: development of a novel interconnection scheme and laser-based patterning processes, in *2021 IEEE 48th Photovoltaic Specialists Conference (PVSC)* (2021), pp. 2539–2543
6. C. Schultz, Laser patterning of chalcopyrite and perovskite based solar cells: Investigation of the laser-material interaction and laser-induced damages, PhD thesis, Technische Universität Berlin (2021), pp. 1–246
7. C. Schultz, A. Bartelt, C. Junghans, W. Becker, R. Schlatmann, B. Stegemann, Enhanced recombination next to laser-patterned lines in CIGSe solar cells revealed by spectral and time-resolved photoluminescence, Appl. Surface Sci. **536**, 147721 (2021)
8. C. Schultz, M. Fenske, J. Dagar, A. Zeiser, A. Bartelt, R. Schlatmann, E.L. Unger, B. Stegemann, Ablation mechanisms of nanosecond and picosecond laser scribing for metal halide perovskite module interconnection − an experimental and numerical analysis, Solar Energy **198**, 410 (2020)
9. B. Stegemann, C. Schultz, Laser patterning of thin films, Digital Encyclopedia of Applied Physics (2019), https://doi.org/10.1002/3527600434.eap830
10. M. Fenske, C. Schultz, J. Dagar, F.U. Kosasih, A. Zeiser, C. Junghans, A. Bartelt, C. Ducati, R. Schlatmann, E.L. Unger, B. Stegemann, Improved electrical performance of perovskite photovoltaic mini-modules through controlled PbI_2 formation using nanosecond laser pulses for P3 patterning, Energy Technol. **9**, 2000969 (2021)
11. J. Dagar, G. Paramasivam, C. Klimm, M. Fenske, C. Schultz, R. Schlatmann, B. Stegemann, E. Unger, Stability assessment of p-i-n perovskite photovoltaic mini-modules utilizing different top metal electrodes, Micromachines **12**, 423 (2021)
12. S.S. Schmidt, C. Wolf, H. Rodriguez-Alvarez, J.-P. Bäcker, C.A. Kaufmann, S. Merdes, F. Ziem, M. Hartig, S. Cinque, I. Dorbandt, C. Köble, D. Abou-Ras, R. Mainz, R. Schlatmann, Adjusting the Ga grading during fast atmospheric processing of $Cu(In,Ga)Se_2$ solar cell absorber layers using elemental selenium vapor, Progr. Photovolt.: Res. Appl. **25**, 341 (2017)
13. J.M. Liu, Simple technique for measurements of pulsed Gaussian-beam spot sizes, Opt. Lett. **7**, 196 (1982)
14. P.J. Potts, *A Handbook of Silicate Rock Analysis* (Chapman and Hall, New York, NY, 1986)
15. B. Stegemann, M. Schüle, C. Schultz, K. Stelmaszczyk, M. Weizman, C. Wolf, C.A. Kaufmann, B. Rau, R. Schlatmann, F. Fink, Electrical and structural functionality of CIGSe solar cells patterned with picosecond laser pulses of different wavelengths, in *2015 IEEE 42nd, IEEE Photovoltaic Specialist Conference (PVSC)* (2015), pp. 1–4
16. C. Schultz, M. Schuele, K. Stelmaszczyk, M. Weizman, O. Gref, F. Friedrich, C. Wolf, N. Papathanasiou, C.A. Kaufmann, B. Rau, Laser-induced local phase transformation of CIGSe for monolithic serial interconnection: analysis of the material properties, Sol. Energy Mater. Sol. Cells **157**, 636 (2016)
17. B. Stegemann, M. Schüle, C. Schultz, K. Stelmaszczyk, M. Weizman, C. Wolf, C.A. Kaufmann, B. Rau, R. Schlatmann, F. Fink, Picosecond and nanosecond laser structuring of CIGSe solar cells, in *Proc. 6th World Conf. Photovolt. Energy Convers.* (2014), pp. 319–320
18. K. Brecl, M. Topič, F. Smole, A detailed study of monolithic contacts and electrical losses in a large-area thin-film module, Progr. Photovolt.: Res. Appl. **13**, 297 (2005)
19. D. Thomas, In situ Spannungs- und Strukturanalyse von Molybdän- und $CuInS_2$-Dünnschichten mittels Röntgendiffraktion, PhD thesis, Technische Universität Berlin, (2012), pp. 1–138
20. M. Domke, G. Heise, I. Richter, S. Sarrach, H.P. Huber, Pump-probe investigations on the laser ablation of CIS thin film solar cells, Phys. Procedia **12**, 396 (2011)
21. G. Heise, M. Englmaier, C. Hellwig, T. Kuznicki, S. Sarrach, H.P. Huber, Laser ablation of thin molybdenum films on transparent substrates at low fluences, Appl. Phys. A **102**, 173 (2011)
22. Y.G. Shen, Effect of deposition conditions on mechanical stresses and microstructure of sputter-deposited molybdenum and reactively sputter-deposited molybdenum nitride films, Mater. Sci. Eng. A **359**, 158 (2003)
23. G. Heise, M. Domke, J. Konrad, S. Sarrach, J. Sotrop, H.P. Huber, Laser lift-off initiated by direct induced ablation of different metal thin films with ultra-short laser pulses, J. Phys. D: Appl. Phys. **45**, 315303 (2012)
24. C. Schultz, M. Schüle, K. Stelmaszczyk, J. Bonse, R. Witteck, M. Weizman, H. Rhein, B. Rau, R. Schlatmann, V. Quaschning, Film side laser patterning of molybdenum thin films sputter-deposited onto glass, in *27th European Photovoltaic Solar Energy Conference and Exhibition* (2012), pp. 2266–2272
25. A. Wehrmann, S. Puttnins, L. Hartmann, M. Ehrhardt, P. Lorenz, K. Zimmer, Analysis of laser scribes at CIGS thin-film solar cells by localized electrical and optical measurements, Opt. Laser Technol. **44**, 1753 (2012)
26. P.-O. Westin, J.T. Wätjen, U. Zimmermann, M. Edoff, Microanalysis of laser micro-welded interconnections in CIGS PV modules, Sol. Energy Mater. Sol. Cells **98**, 172 (2012)
27. P.O. Westin, U. Zimmermann, M. Edoff, Laser patterning of P2 interconnect via in thin-film CIGS PV modules, Sol. Energy Mater. Sol. Cells **92**, 1230 (2008)
28. G. Heise, A. Heiss, H. Vogt, H.P. Huber, Ultrafast lasers improve the efficiency of CIS thin film solar cells, Phys. Procedia **39**, 702 (2012)
29. C. Schultz, M. Fenske, J. Dagar, G.A. Farias Basulto, A. Zeiser, A. Bartelt, C. Junghans, R. Schlatmann, E. Unger, B. Stegemann, Laser-based series interconnection of chalcopyrite und perovskite solar cells: analysis of material modifications and implications for achieving small dead area widths, Mater. Today: Proc. **53**, 299 (2021)

Cite this article as: Christof Schultz, Guillermo Antonio Farias Basulto, Nicolas Otto, Janardan Dagar, Andreas Bartelt, Rutger Schlatmann, Eva Unger, Bert Stegemann, Laser-based monolithic series interconnection of two-terminal perovskite-CIGSe tandem solar cells: determination of the optimal scribe line properties, EPJ Photovoltaics **14**, 16 (2023)